A DESIGN STUDY OF ILC ELECTRON DRIVEN POSITRON SOURCE

Masao Kuriki *, Hiroki Tajino, Shun Konno, Zachary Liptak, Tohru Takahashi,
Graduate School of Advanced Science and Engineering, Hiroshima U.
Kaoru Yokoya, Junji Urakawa, Tsunehiko Omori,
High Energy Accelerator Research Organization

Abstract

ILC is an electron-positron linear collider based on Super-conducting linear accelerator. Linear collider is the only solution to realize high energy electron-positron collision beyond the limit of synchrotron radiation energy loss by ring colliders. Because the beam current of injector of linear colliders is much larger than that of ring colliders since the beam is not reusable, providing an enough amount of particles, especially positron is a technical issue. In this article, we present a design of electron driven positron source for ILC, especially how to accelerate stably the high current beam by compensating the heavy beam loading to obtain a beautiful multi-bunch positron beam.

INTRODUCTION

ILC is an e+e- linear collider with center of mass energy 250 GeV - 1000 TeV [1] employing Super-conducting accelerator. One pulse contain 1312 bunches with 4.8 nC charge including 50% margin and the pulse is repeated with 5 Hz resulting the average beam current 21 A. This is a technical challenge, because the amount of positron per second is 40 times larger than that in SLC [2], which was the first linear collider. The configuration of the positron source is schematically shown in Fig. 1. The positron generated by electron beam is captured and boosted up to 5 GeV. The drive beam energy is 3.0 GeV electron. The generated positron is captured in RF bucket by L-band Standing Wave (SW) cavities with 0.5 Tesla solenoid field; This is Capture Linac. The positron is further accelerated up to 5 GeV by L-band and S-band Traveling Wave (TW) cavities (Booster) followed by ECS (Energy Compression Section).

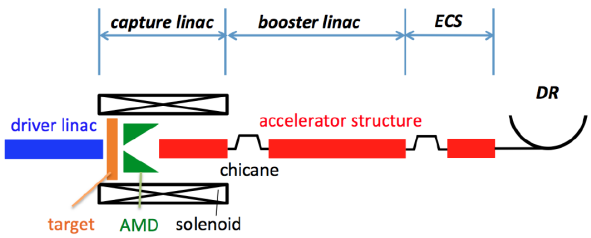

Figure 1: Configuration of E-Driven ILC positron source is schematically shown.

Generating positron in the pulse format of the main linac, 1312 bunches with 545 ns, might cause a severe damage on the production target, since 1312 bunches are concentrated in a small spot size. To relax the energy deposition density on the target, the target has to be rotated with 400 m/s tangential speed which is faster than speed of sound in air. To solve this problem, the positron is generated with 20 pulses and one pulse contain 66 bunches in our scheme as shown in Fig. 2. In this case, the energy density on the target is 20 times less and the spot of each pulse can be shifted easily with a slow rotation, 5 m/s in our design [3]. The speed is slower than a professional marathon runner. The pulse is repeated in 300 Hz and the system is based on the normal conducting accelerator. It takes 63 ms to generate 1312 bunches of positron and the generated positron is stored in DR until the accelerating in the main linac. The pulse structure in the main linac can be controlled by the beam extraction from DR, which is independent from that in the positron source.

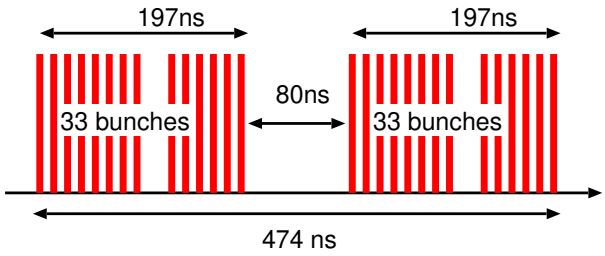

Figure 2: The beam structure in the positron source. Each mini-train contains 33 bunches.

The design was progressed improving the reality of the simulation [3–6] and finally the beam loading and its compensation is now included. For those simulations, the peak energy deposition density on the target is kept less than 35 J/g [7], which is considered to be a practical limit of the safety operation. To obtain uniform intensity positrons over the pulse, the transient variation of the acceleration field by the beam loading has to be compensated so that positrons are accelerated uniformly. Compensation for the transient beam loading by Phase Modulation (PM) on the input RF was proposed by Urakawa [8,9]. The detail study of the compensation is discussed in Ref. [10, 11]. In this article, we present the electron driven ILC positron source accounting this effect.

ELECTRON DRIVER

3 GeV electron driver is composed from 2600 MHz (S-band) normal conducting TW cavity. The cavity is originally designed for ATF(Accelerator Test Facility) at KEK [12] in 2856 MHz and the parameters are scaled to 2600 MHz. As a basic unit, 4 cavities are driven by two klystrons with 80 MW peak power. Accounting 10 % power loss in RF wave guide, the input power to one cavity is 36 MW. The shunt impedance is 57.2 M/m with L=3.228 m and the attenuation τ is 0.57 resulting 0.91 s filling time.

* mkuriki@hiroshima-u.ac.jp

Energy fluctuation by the transient beam loading is compensated by amplitude modulation (AM) on the input RF [11]. A perfect compensation is possible with two components AM, a step pulse and a trapezoidal pulse. In this case, a high peak power is required at the vertex of the trapezoidal modulation and the acceleration field becomes less. In this design study, we employ one component AM with a step pulse to revive the average acceleration field allowing for some variation. E_0 is the initial cavity field, and E_1 is the amplitude of AM. E_1 is determined as

$$E_1 = \frac{rI}{2}\left(\frac{-\omega/Qt_p e^{-2\tau}}{1-e^{-\omega/Qt_p}} + 1\right), \quad (1)$$

where t_p is the pulse length setting the same cavity voltage at $t = t_f$ and $t = t_f + t_p$. The initial field E_0 is determined as

$$P_{max} = \frac{L}{r(1-e^{-2\tau})}(E_0 + E_1)^2 \quad (2)$$

where P_{max} is the maximum input RF power.

Figure 3 shows the temporal evolution of the cavity voltage with AM. The acceleration voltage per cavity is 31.9 ± 0.4 MV with 0.65 A beam loading current I_B with 36 MW input power. The error is the variation in RMS by the transient beam loading. The first two cavities are driven by two klystrons, so that the input power per cavity is 72 MW resulting 43.5 ± 0.6 MV with the same I_B. The electron driver is composed from two cavities as the injector and 100 cavities as the normal section. The total beam energy is 3.3 GeV which has 10% margin. The lattice of the electron driver is summarized in Table 1.

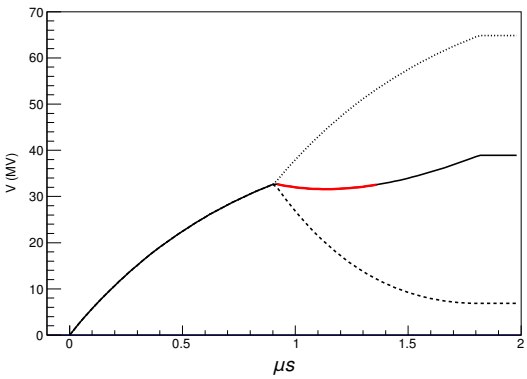

Figure 3: Accelerating voltage evolution of the 3m S-band cavity with the one-component AM with 0.65 A beam loading current. The red solid line shows the beam duration. The solid line, dotted line, and dashed line show the cavity voltage, the RF voltage, and the beam loading voltage, respectively.

TARGET AND MAGNETIC FOCUSING

Target is a rim with 500 mm diameter and 16 mm thickness made from tungsten-rhenium alloy. To avoid overlapping of the pulse on the target, it is rotated with 5 m/s tangential speed. At the down stream of the target, a flux concentrator as a magnetic focusing to suppress the transverse momentum is placed. The detail of those arrangements is presented in Ref. [6]. The loading on the target is evaluated by PEDD (Peak Energy Deposition Density in J/g); the W-Re destruction limit is 76 J/g [13], and the safe operating threshold is considered to be 35 J/g [6]. The positron production yield is 1.17 as evaluated in , the electron bunch charge is 4.1 nC. PEDD for 4.8 nC electron bunch is 33.6 J/g [6], giving 28.7 J/g for 4.1 nC. This is even lower the threshold.

Table 1: The lattice configuration of the electron driver. The energy and the gain is in MeV. G, Q, and S stand for RF Gun, quadrupole magnet, and S-band cavity.

Section	Lattice	Energy gain	Energy
Pre injector	G + 2S + 3Q	92.0	92.0
Injector #1	4(2Q + S)	127.6	219.6
Injector #2	2(2Q + 2S)	127.6	347.2
Injector #3	2(Q + 2S)	127.6	474.8
Linac #4-#7	4(Q + 4S)	510.4	985.2
Linac #8-#25	18(Q + 4S)	2296.8	3282.0

CAPTURE LINAC

The capture linac is composed from 36 APS (Alternate Periodic Structure) $\pi/2$ mode SW cavity. The structure is 1.3 m long with 21 cells. The shunt impedance is 31.5 M/m. The purpose of the capture linac is to confine the generated positrons in a RF bucket. An effective way for the capturing is the deceleration capture method where positrons are placed on the deceleration phase [14]. The positron is moving to the acceleration phase by phase slipping gradually and the positron is captured at the acceleration phase. Figure 4 shows the captured positron distribution in the longitudinal phase space z and $\delta = (\gamma - \bar{\gamma})/\bar{\gamma}$ where γ and $\bar{\gamma}$ are Lorentz factor and the average. The positrons after acceleration are distributed along the RF curvature.

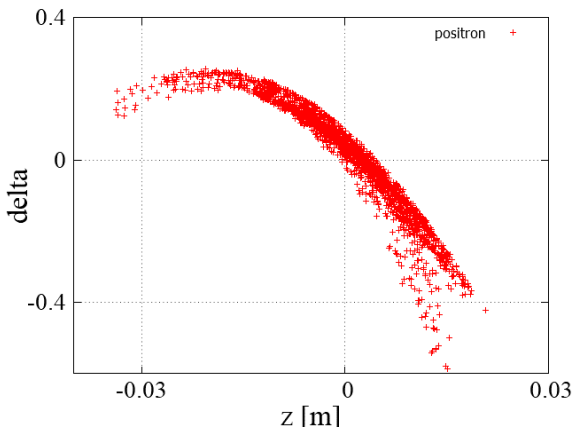

Figure 4: Longitudinal phase space ($z - \delta$) distribution of positron at the end of the capture linac.

In the capture linac, the beam phase is moving over the linac. To compensate the voltage variation by the beam loading, phase modulation (PM) should be introduced. The

detail of the beam loading compensation with PM is described in Ref [11]. We consider a combination of two input RF signals with a constant RF amplitude for PM. The phase of each input RF signals are modulated. If the phase modulation for the two klystrons are the same sign, the phase of the combined RF is modulated. If the anti sign, the amplitude of the output is modulated.

If the phase modulation to RF is instantaneous, the beam loading is compensated perfectly [11]. In reality, however, the klystron is driven by a cavity, which has a finite time constant; even if the phase of the RF input is modulated, the modulation of the klystron output appears with a delay. To evaluate the effect of the delay of PM, we perform the numerical calculation. If there is a delay with τ as the time constant, the input RF evolution is

$$\begin{aligned} \tilde{V_{RF}} &= V_{RF}\{u(t) - u(t-t_b)\} \\ &\quad + V_{RF} e^{-\frac{t-t_b}{\tau}} u(t-t_b) \\ &\quad + V_{RF} u(t-t_b) e^{i\phi} \left(1 - e^{-\frac{t-t_b}{\tau}}\right), \end{aligned} \tag{3}$$

where V_{RF} is the RF voltage amplitude, $u(t)$ is the step function, t_b is time to start the beam acceleration, and ϕ is PM angle. We calculate the cavity response with this modulation. As the klystron Q value, we assume 2000. It can be compared with Q value of APS cavity, 25000. Klystron response is 12 times faster than that of APS cavity. The time constant τ is 0.24s in this case. This Q value of klystron is quite ordinal and further optimization for a faster response is possible, but we assume this value anyway. The cavity voltage is calculated using a coupled pendulum model developed by T. Shintake [15].

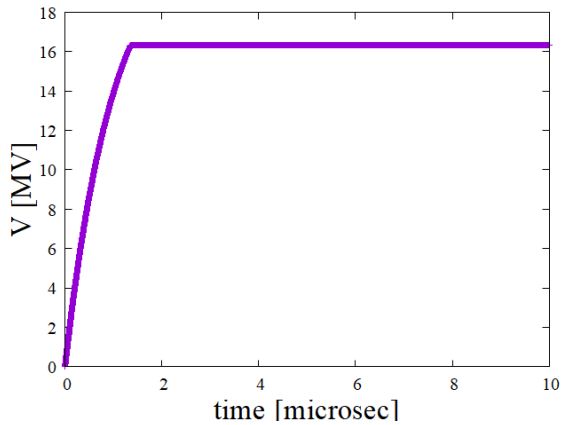

Figure 5: Real part of the cavity voltage evolution with 22.5 MW RF power with 1 A beam loading current starting at the filling time. PM with delay is applied.

Figures 5 and 6 show the cavity voltage evolution with delay of the klystron output according to Eq. (3). Figure 5 and 6 show the real part and the imaginary part, respectively. We start the beam acceleration at the filling time (kink in Fig. 5). The input RF power is 22.5 MW and the beam current is 1 A. The beam angle θ is $\pi/6$. The imaginary part has a small dip as shown in Fig. 5). The amplitude is -0.15 MV. This value should be compared to the real part amplitude, 16 MV. The dip of the imaginary component cause the phase fluctuation of 9.4 mrad, whose impact on the acceleration is limited.

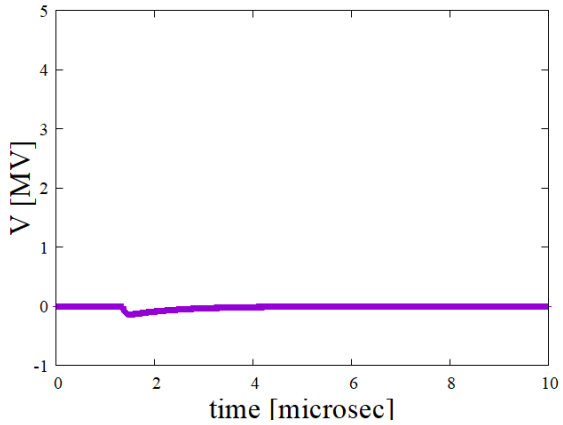

Figure 6: Imaginary part of the cavity voltage evolution with 22.5 MW RF power with 1 A beam loading current starting at the filling time. PM with delay is applied.

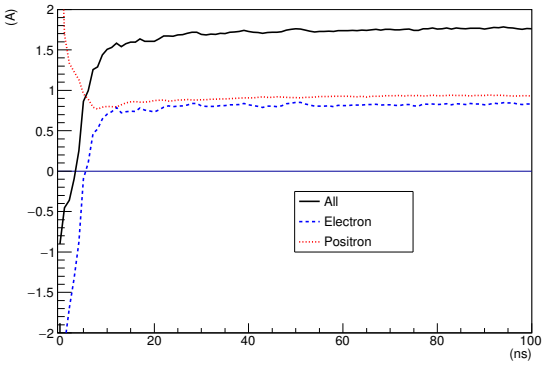

Figure 7: The beam loading current as a function of time in the capture linac. The electron, positron and sum of the current are shown with dotted, dashed, and solid lines, respectively.

Figure 7 shows the beam loading current as a function of time, where the origin of time is when the positron is generated in the target. The electron, positron and sum of the current are shown with dotted, dashed, and solid lines, respectively. Initially, the beam loading current by electron and positron are cancelled, but it rapidly increased because they are captured at "acceleration phase". The acceleration voltage by the cavity is decreased when the beam loading current is increased as shown in Fig. 8.

CHICANE AND BOOSTER LINAC

After the capture linac, a chicane is placed to remove electrons. As a sub-effect, the bunch length is shortened by the momentum compaction factor. The chicane parameter is adjusted as the bunch length after the chicane is minimized as shown in Fig. 9.

The positron booster is composed from L-band [16] and S-band [17] Traveling Wave (TW) cavities. The parameters are summarized in Table 2.

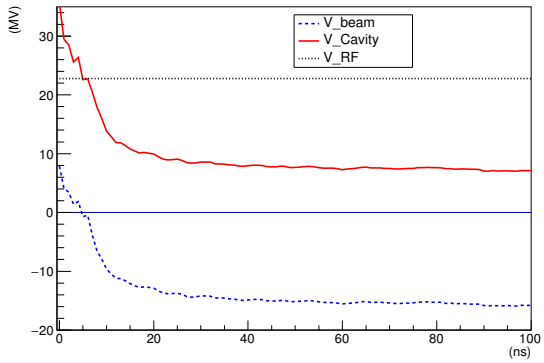

Figure 8: The cavity voltage (solid line), the beam loading voltage (dashed line) and the RF voltage (dotted line) are shown as a function of time.

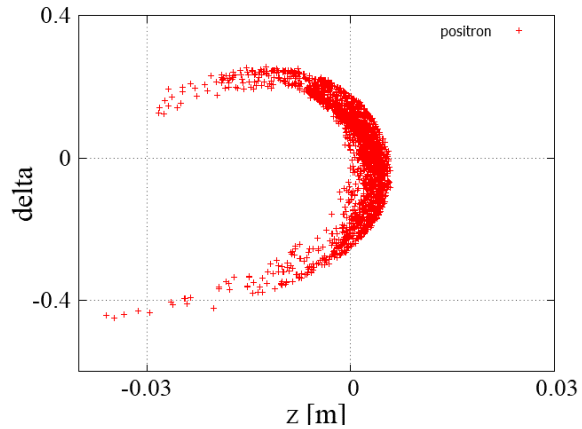

Figure 9: Longitudinal phase space ($z - \delta$) distribution of positron after the chicane.

By assuming 4.8 nC bunch charge, the beam loading current in the booster is 0.78 A. Figure 10 and 11 show the voltage evolution of the L-band and S-band cavities with the beam loading, respectively. The beam loading compensation scheme is identical to that of the S-band TW cavity in the electron driver. The voltage are 16.5 $\pm$ 0.1 MV for L-band cavity and 29.2 $\pm$ 0.6 MV for S-band cavity. Those voltages are evaluated with P_{max} is 22.5 MW for L-band and 36 MW for S-band including 10% power loss by wave guide. Table 3 summarizes the lattice configuration of the booster based on the design in Ref. [4]. As the energy at the booster entrance, 250 MeV is assumed.

Table 2: Parameters of L-band and S-band TW Cavities in the Booster

Parameter	L-band	S-band	unit
Shunt impedance	46.5	55.1	M/m
Length	2.00	1.96	m
Aperture (2a)	35.0 39.4	24.3-20.3	mm
Attenuation τ	0.261	0.333	
Filling time t_f	1.28	0.55	s

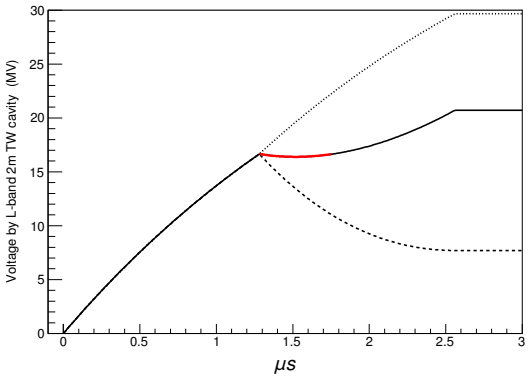

Figure 10: The voltage evolution of the L-band 2m TW cavity with 22.5 MW RF input and 0.78 A beam loading current is shown with the same manner as those in Fig. 3.

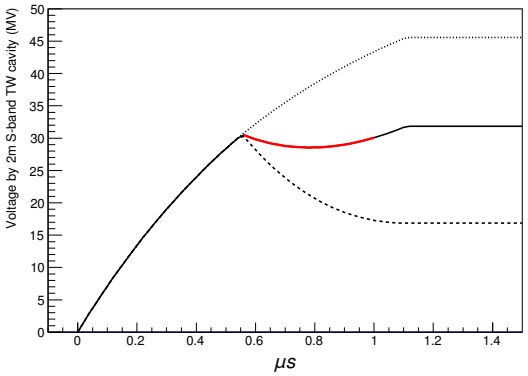

Figure 11: The voltage evolution of the S-band 2m TW cavity with 36 MW RF input and 0.78 A beam loading current is shown with the same manner as those in Fig. 3.

ECS AND POSITRON YIELD

The purpose of ECS is to compress the energy spread of positron after the booster, down to $\pm$0.75%, within DR (damping ring) acceptance. ECS is composed from three chicane (18.6m, 55.8 m in total) and 4 L-band 3m TW cavities (4Q+4L lattice, 22.4 m) driven by 4 klystrons. Other two L-band 3m TW cavities (2L, 6.4 m) driven by two klystrons are set for the beam loading compensation.

The positron yield is defined as the number of positrons obtained in DR dynamic aperture (acceptance) per electrons

Table 3: Lattice configuration of the booster. In addition to the abbreviation in Table 1, L stands for L-band TW cavity. The gain is the acceleration energy in the section and Energy is the beam energy at the end of the section in MeV.

Lattice	unit #	# of cavity	Energy gain	Energy
4Q+1L	3	12	198	448
4Q+2L	15	60	990	1438
4Q+4L	18	72	1188	2626
4Q+4S	25	100	2860	5486

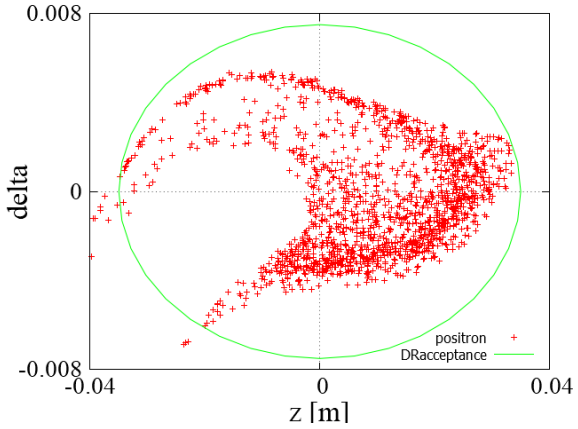

Figure 12: Longitudinal phase space ($z - \delta$) distribution of positrons after ECS section. R_{56} of ECS is -1.04. The solid circle shows DR acceptance.

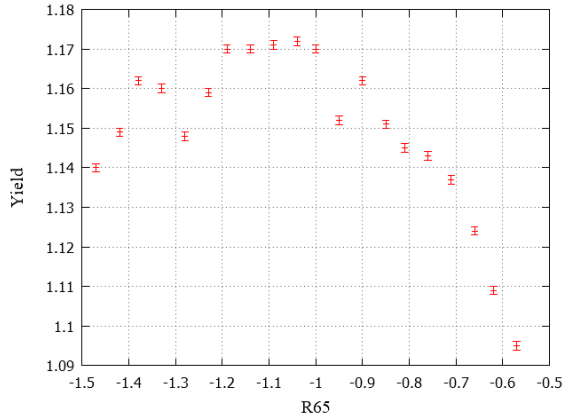

Figure 13: Positron yield as a function of R_{65} of ECS. R_{56} is optimized for each R_{65}.

on the production target. The DR acceptance is [1]

$$\gamma A_x + \gamma A_y < 0.07 \text{ m}, \quad (4)$$

$$\left(\frac{z}{0.035}\right)^2 + \left(\frac{\delta}{0.0075}\right)^2 < 1.0. \quad (5)$$

Figure 12 shows the longitudinal phase space distribution after ECS with DR acceptance (solid circle). Figure 13 shows positron yield as a function of R_{65} of ECS. R_{56} is optimized for each R_{65}. Yield is 1.17 and uniform in region of $-1.2 < R_{65} < -1$.

SUMMARY

According to detail studies of the beam loading compensation for SW and TW cavities, the acceleration field is determined. Based on those parameters, the number of RF units and the lattice are fixed and the ILC E-Driven positron source design is established. The evaluated positron yield was 1.17 giving the electron intensity on the target satisfying the safety condition.

ACKNOWLEDGEMENTS

This work is partly supported by Grant-in-Aid for Scientific Research (B) and US-Japan Science and Technology Cooperation Program in High Energy Physics.

REFERENCES

[1] "ILC Technical Design Report", Rep. KEK-Report, 2013.

[2] "SLC Design Report", Rep. SLAC-R-714, 1984.

[3] T. Omori *et al.*, "A conventional positron source for international linear collider", *Nucl. Instr. and Meth. A*, vol. 672, no. 52, 2012. doi:10.1016/j.nima.2011.12.032

[4] Y. Seimiya *et al.*, "Positron capture simulation for the ILC electron-driven positron source", *Prog. Theor. Exp. Phys.*, vol. 2015, no. 10, Oct. 2015. doi:10.1093/ptep/ptv136

[5] M. Kuriki *et al.*, "Electron Driven ILC Positron Source with a Low Gradient Capture Linac", in *Proc. LINAC'16*, East Lansing, MI, USA, Sep. 2016, pp. 430–433. doi:10.18429/JACoW-LINAC2016-TUPRC008

[6] H. Nagoshi, M. Kuriki *et al.*, "A design of an electron driven positron source for the international linear collider", *Nucl. Instr. and Meth. A* vol. 953, p. 163134, 2020. doi:10.1016/j.nima.2019.163134

[7] T. Takahashi, "Radiation effect on the target and capture devices", in *Proc. of LCWS2018*, Arlington, Texas, USA, Oct. 2018.

[8] M. Kuriki *et al.*, "Beam Loading Compensation of APS Cavity with Off-Crest Acceleration in ILC e-Driven Positron Source", in *Proc. IPAC'21*, Campinas, Brazil, May 2021, pp. 1368–1371. doi:10.18429/JACoW-IPAC2021-TUPAB015

[9] M. Kuriki *et al.*, "A study of beam loading effect ant its compensation on Alternate Periodic Structure Cavity on E-Driven ILC Positron Source ", in *Proc. of PASJ2021*, Takasaki, Japan, Aug. 2021, paper MOP031.

[10] M. Kuriki, "Energy Spread Compensation in Arbitrary Format Multi-Bunch Acceleration With Standing Wave and Traveling Wave Accelerators", in *Proc. IPAC'18*, Vancouver, Canada, Apr.-May 2018, pp. 307–310. doi:10.18429/JACoW-IPAC2018-MOPMF076

[11] M. Kuriki *et al.*, "Beam Loading Compensation of Standing Wave Linac with Off-Crest Acceleration", in *Proc. IPAC'22*, Bangkok, Thailand, Jun. 2022, pp. 1893–1896.

[12] "ATF Design and study report", KEK Internal 95-4, 1995.

[13] S. Ecklund, "Positron target materials tests", Rep. SLAC-CN-128, 1981.

[14] M. James *et al.*, "A new target design and capture strategy for high-yield positron production in electron linear colliders", *Nucl. Instr. and Meth. A*, vol. 307, pp. 207-212, 1991.

[15] T. Shitake, *Proc. of Joint US-CERN-Japan International School*,ISBN981-02-3838-X(1996).

[16] K. Saito *et al.*, "Design of L-band Positron Capture Accelerating Structure", in *Proc. of PASJ2010*, 2010, paper WEPS069.

[17] S. Matsumoto, T. Higo, K. Kakihara, T. Kamitani, and M. Tanaka, "Large-aperture Travelling-wave Accelerator Structure for Positron Capture of SuperKEKB Injector Linac", in *Proc. IPAC'14*, Dresden, Germany, Jun. 2014, pp. 3872–3874.